Concomitant Organic−Inorganic UV-Curing Catalyzed by Photoacids

Abraham Chemtob,[†] Davy-Louis Versace,[†] Cindy Belon,[†] Céline Croutxé-Barghorn,*[,†] and Séverinne Rigolet[‡]

Department of Photochemistry, CNRS UMR 7525, University of Haute-Alsace, ENSCMu, 3, rue Alfred Werner, 68093 Mulhouse Cedex, France, and Laboratoire de Matériaux à Porosité Contrôlée, CNRS UMR 7016, University of Haute-Alsace, ENSCMu, 3, rue Alfred Werner, 68093 Mulhouse Cedex, France

Received May 6, 2008; Revised Manuscript Received July 17, 2008

ABSTRACT: Organic−inorganic UV-curing of organosilanes containing epoxy and trialkoxysilyl functional groups in the same monomer was implemented using a diaryl iodonium salt as cationic photoinitiator. UV-generated Brönsted acids through photolytic degradation were found to be effective in catalyzing both epoxy ring-opening polymerization and alkoxysilane sol−gel polycondensation reactions. Competition between the formation of inorganic and organic phases was kinetically studied using real-time Fourier transform infrared spectroscopy (RT-FTIR). The nature of the hybrid monomer, the effect of changing the film thickness, the type of substrate and the influence of laminated conditions on the polymerization kinetics were assessed. ^{29}Si and ^{13}C solid state NMR measurements were also performed to investigate the structure of the UV-cured hybrid materials.

Introduction

Polymer nanocomposite science is a very dynamic and emerging field in polymer chemistry. Like other polymerization processes, photopolymerization has known a recent explosion of research in this area.[1] UV-cured organic−inorganic hybrid materials generally attempt at combining hardness, flexibility and resistance to chemicals, scratch, heat, while maintaining transparency and gloss.[2] Major applications in this field are abrasion resistant coatings,[3] protective films for plastics providing barrier properties,[4] glass coatings[5] and novel optical devices.[6] Three synthetic pathways have been mainly developed for the preparation of UV-curable nanocomposites:[7]

(1) The first method relies on low molecular weight organoalkoxysilanes $R'Si(OR)_3$ as one or more of the precursors for the sol−gel reaction, with R′ a photopolymerizable organic function via radical or cationic means. A preliminary sol−gel step produces a liquid organic-based polysiloxane network that can be photopolymerized subsequently, affording a solid cross-linked organic−inorganic system.[8−15]

(2) The second strategy uses preformed inorganic nanoparticles which are dispersed into photocurable monomers. A great deal of examples lie on photoinduced polymerization of multifunctional acrylates incorporating either colloidal or fumed silica.[16−21] In addition to SiO_2, the influence of other equiaxed nanoparticule fillers[22−24] (TiO_2, Al_2O_3, ZnO, etc.) and platelike nanofillers[25−29] (smectic clays or phyllosilicates) have been evaluated within various UV-curing formulations.

(3) More recently, a last approach describes the in situ synthesis of noble metal nanoparticles into a polymer matrix through a UV photoreduction process.[30,31] In particular, silver[32] and gold[33] nanoparticle polymer composites have been reported by a photoinduced electron transfer and UV polymerization occurring simultaneously. Applications in optoelectronics and the fabrication of sensor devices are targeted with these new hybrid photomaterials.

In this work, a novel one-step methodology for preparing hybrid sol−gel coatings has been investigated by UV irradiation of simple and commercial bifunctional hybrid precursors $R'Si(OR)_3$, bearing both an organic epoxy function and alkoxysilane moieties, in presence of an aryl iodonium salt catalyst. Through the in situ liberation of protic acids via onium salt photolysis, polymerization of epoxy takes place concomitantly with hydrolysis and condensation of the reactive silanes. This straightforward method gives access to a stable, solvent-free and single-component hybrid coating composition, which can be applied at room temperature and cured upon UV exposure. For an effective initiation of the sol−gel process, the presence of a catalytic amount of moisture has been found to be necessary.

While oxirane is a classical cationically photopolymerizable function, it is not the case of hydrolyzable alkoxysilyl groups. Very few studies addressing the sol−gel process catalyzed by photoinduced protic acids have been indeed reported in the literature. As early as 1978, Fox et al. were the first to evidence the catalytic activity of onium salts on alkoxysilyl functions upon UV exposure.[34] More recently, photoactivated cross-linking of compounds including alkoxysilanes was described in several patents as a way to produce novel "moisture curable" coatings[35−37] and inks.[38] However, the relationship between the UV-generated photoacids and the resulting inorganic network remained ill-defined. In 2005, Kowalewska moved forward by describing the structure of an oxo-silica network formed during the cross-linking of an alkoxysilyl-modified disiloxane in the presence of various photoacids.[39]

Even less attention has been given so far to the potentialities offered by concomitant curing of the organic and inorganic phases by UV-generated Brönsted acids. Its feasibility was first demonstrated in 1995 by Crivello et al. who described the UV irradiation of an "ambifunctional" monomer having both epoxycyclohexyl and trimethoxysilyl reactive functional groups.[40] In the presence of a cationic triarylsulfonium catalyst, a rapid polymerization of the epoxy groups was observed, followed by a slow consumption of the trialkoxysilyl groups, without further investigations. Subsequently to these earlier efforts, Soucek et al. carried out the UV illumination of an organic epoxidized linseed oil mixed with either a siloxane oligomer based on tetraethoxysilane (TEOS) or titanium isopropoxide. The presence of sulfonium salt enabled in this case both a ring-opening of the organic resin and the formation of the inorganic network.[41,42] Sangermano et al. also contributed to the subject by investigating the dual UV curing of a series of hybrid systems comprising a

* Corresponding author. E-mail: Celine.Croutxe-Barghorn@uha.fr. Tel: + 33 3 8933 5017. Fax: + 33 3 8933 5014.
[†] Department of Photochemistry, CNRS UMR 7525.
[‡] Laboratoire de Matériaux à Porosité Contrôlée, CNRS UMR 7016.

10.1021/ma801017k CCC: $40.75
Published on Web 10/02/2008

Table 1. Structure of the Bifunctional Hybrid Monomers and the Cationic Photoinitiator

COMPOUND	FUNCTION	STRUCTURE
2-(3,4-Epoxy-cyclohexylethyl)trimethoxysilane TRIMO	Hybrid monomer	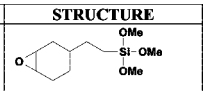
(3-Glycidyloxypropyl) trimethoxysilane GPTMS	Hybrid monomer	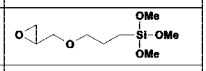
(4-Methylphenyl)[4-(2-methylpropyl) phenyl] iodonium hexafluorophosphate I 250 (Ciba Specialty Chemicals)	Photoinitiator	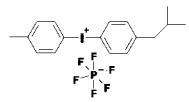

reactive organic resin and various epoxy or vinylether alkoxysilane precursors.[43−45] Despite these developments, the dual organic−inorganic curing initiated by UV-generated Brönsted acids is still in its infancy. This lack of understanding prompted us to examine more closely the photo-cross-linking of two basic "hybrid" precursors containing cationically polymerizable epoxy and trialkoxysilyl functional groups in the same monomer (GPTMS and TRIMO, Table 1) in the presence of diaryl iodonium salt.

The first part focuses on the organic and inorganic photopolymerization kinetics using real-time Fourier transform infrared spectroscopy (RT-FTIR). In our case, a competition is likely to occur between hydrolysis−polycondensation reactions involving the trialkoxysilyl functions and the epoxy ring-opening cationic photopolymerization. In a second part, a particular effort was made to understand how the hybrid structure is affected by the two concurrent polymerization processes. For this, the hybrid network microstructure was characterized by ^{29}Si and ^{13}C NMR spectroscopy. In addition, a set of experimental parameters influencing the dual polymerization process have been thoroughly investigated. The monomer structure, the film thickness, the type of substrate and the laminated conditions have been proven to display a critical effect on the structure of the composite materials. A last part was devoted to the thermal characterization and stability of these novel organic−inorganic coatings through dynamic scanning calorimetry (DSC) and thermogravimetric analysis (TGA).

Experimental Section

Materials. 3-(Glycidyloxypropyl)trimethoxysilane (GPTMS) and [2-(3,4-epoxycyclohexyl)ethyl] trimethoxysilane (TRIMO) were purchased from Gelest and used without further purification. (4-Methylphenyl)[4-(2-methylpropyl) phenyl] iodonium hexafluorophosphate (I 250 or Irgacure 250), which behaves as a photoinitiator for both the organic and inorganic moieties of the hybrid monomers, was provided by Ciba Specialty Chemicals. I 250 is a 75% solution of the active substance in propylene carbonate. Byk 333 supplied by BYK Chemie is a surface wetting agent based on a polyether modified polydimethylsiloxane. The structures of the respective monomers and photoinitiator are shown in Table 1.

Polymerizations. The photoinduced inorganic−organic polymerization of organosilanes was performed by mixing GPTMS (or TRIMO) with 2 wt % of I 250 and 0.5 wt % of Byk 333. The homogeneous formulation was then applied by means of a bar coater to form a 15 μm thick liquid film layer. A set of bar coaters ranging from 4 to 50 μm was implemented in the part devoted to the effects of film thickness. Two types of UV irradiation equipment were used to perform a curing of the nanocomposite formulation. The first one was a Lightningcure LC8 (L8251) from Hamamatsu equipped with a mercury−xenon lamp (200 W) coupled with a flexible light-guide. The end of the optical guide was placed at a distance of 3 cm from the sample and directed at an incident angle of 90° onto the sample window. This illumination equipment was used for the kinetic analysis of the polymerization by RT-FTIR spectroscopy. In IR experiments, samples were deposited onto a barium fluoride crystal, and all photopolymerizations were performed at room temperature with an intensity of 180 mW/cm^2 during 210 s corresponding to a light dose of 37.8 J/cm^2. The second type of irradiation device is a Minicure UV conveyor system from Nordson equipped with a medium pressure mercury lamp (electrical power of 120 W/cm) and a semielliptic reflector. The belt conveyor was operated at a belt speed of 5 m/min, which corresponds to an exposure time of 1.2 s per pass under the lamp. The maximum UV-light intensity at the sample position was measured by radiometry (International Light Radiometer IL-390) to be 3.3 J/cm^2 bypass in the 250−400 nm wavelength range covered by this apparatus. In this case, the UV-curable organosilane was deposited on a glass plate at a thickness of 15 μm and exposed to UV irradiation by 10 successive passes. This number of passes was chosen to provide the sample with a light dose close to that yielded by the first irradiation device, approximately 33 J/cm^2. The resulting hard and solid UV cross-linked samples were used subsequently in solid state NMR analysis, DSC and TGA measurements.

The conventional sol−gel polymerization of the trialkoxysilanes was carried out in bulk at ambient temperature in presence of an acidified water solution of HCl. A water to silicon ratio (r_w) of 3 and an acid concentration of 0.1 mol/L were chosen. The mixture was allowed to mature for 72 h to permit a partial elaboration of the silicate backbone. Transparent and low viscosity liquids were obtained whatever the precursor employed. The sols were then analyzed by liquid ^{29}Si NMR to determine their degree of condensation.

Methods. The photochemical process taking place under illumination was followed by RT-FTIR spectroscopy. Infrared spectra were recorded with a Bruker Vertex 70 FTIR spectrometer equipped with a liquid-nitrogen-cooled mercury−cadmium telluride detector. Infrared spectra were collected at a resolution of 4 cm^{-1}. For the Fourier transformation of the interferogram, a Blackman-Harris-3-term apodization function was selected as well as a zerofilling factor of 2 and a standard Mertz procedure for phase correction. Data acquisition was performed using a double sided forward/backward. Three polymerizations were carried out for each kinetic study, and the resulting data were then averaged. During UV irradiation, the absorbance decrease of the C−H epoxy stretching vibration band at 3050 cm^{-1} was exploited to monitor epoxy conversion in all the GPTMS samples. In TRIMO-based samples, the antisymmetrical ring stretching at 885 cm^{-1} was selected. To evaluate the extent of the sol−gel process during the UV illumination of both monomers, the formation of −OH groups was followed by the ratio

$$\frac{\text{intensity of the band at 3400 cm}^{-1}}{\text{intensity of the reference band at 1193 cm}^{-1}\ (t=0)} \times 100 \text{ (arbitrary units)} \quad (1)$$

The OH groups have a characteristic absorption band at 3400 cm^{-1}. The band at 1193 cm^{-1} assigned to Si−CH$_2$ stretching was chosen to obtain a normalized intensity of the band at 3400 cm^{-1}. This latter provides a valuable insight into the Si−OH formation/consumption by hydrolysis/condensation reactions.

Liquid and solid state NMR measurements were recorded at room temperature in all cases.

(1) ^{29}Si Liquid NMR experiments (Larmor frequency: 79.48 MHz) were performed on a Bruker Avance II 400 spectrometer operating at B_0 = 9.4 T with a Bruker BBO probe. A π/4 pulse duration of 6.7 μs and a 12 s (7 s) recycling delay for GPTMS (TRIMO) were chosen. ^{29}Si spin lattice relaxation times (T_1) were measured with the saturation-recovery pulse sequence: 33.6 and 18.5 s respectively in GPTMS and TRIMO-based sols. These recording conditions are meant to ensure the quantitative determination of the proportions of the different Si species. Sols produced by conventional sol−gel polymerization of the trialkoxysilanes were first introduced in an 8 mm tube. This latter was then inserted into a 10 mm tube containing $CDCl_3$ as an internal lock and tetramethylsilane as a reference. Through such a method, sols can be scanned without affecting their microstructure. 60 scans were

accumulated for each spectrum. Deconvolution of the ^{29}Si spectra with the dmfit software[46] gives the quantitative determination of the proportions of the T^n Si substructures.

(2) ^{13}C Liquid NMR experiments were measured at 75.45 MHz on Bruker Advance 300 using $CDCl_3$ as an internal reference. These recording conditions allowed the determination of the ^{13}C spectra of the organosilane monomers.

(3) In a view to obtain quantitatively reliable ^{29}Si (and ^{13}C) data for the UV cross-linked materials, single pulse magic angle spinning (SPE-MAS) experiments have been performed on a Bruker Avance II 400 spectrometer with a Bruker double channel 7 mm probe. For this, zirconium rotors were employed at 79.48 MHz (100.6 MHz) using a pulse angle of $\pi/4$, a recycling delay of 80 s (60 s), a spinning frequency of 4 kHz and high-power proton decoupling during the acquisition. ^{29}Si and ^{13}C chemical shifts are both relative to tetramethylsilane.

Coating thickness was determined using an Altisurf 500 workstation (ALTIMET) equipped with a 350 μm AltiProbe optical sensor using a working speed set at 100 Hz. To perform the measurements, the formulation was coated onto a BaF_2 pellet, leaving a part of the substrate uncoated so that the height of the coating can be determined. Thermogravimetric measurements (TGA) were run on a Setaram Labsys thermoanalyzer under air flow conditions. A temperature range from 20 °C up to 1000 °C was scanned at a heating rate of 5 °C/min. The differential scanning calorimetry (DSC) thermograms were obtained with a Q 200 modulated DSC (TA Instruments) under N_2 flow in the temperature ranges: 2 to 300 °C (first and second heating). In these experiments, sample masses ranging between 3.2 and 4.9 mg were introduced in aluminum hermetic pans and heated/cooled at a rate of 10 °C/min.

Results and Discussion

I. Dual UV-Curing Kinetics of Epoxy Trialkoxysilane Hybrid Monomers. As a preliminary step, storage stability of the GPTMS and TRIMO-based silanes with the diaryl iodonium salt was assessed by RT-FTIR and ^{13}C CP MAS NMR. The structures of these different compounds are given in Table 1. Neither sign of early hydrolysis nor ring-opening of the epoxy groups was detected over one week, thus confirming the absence of photolytic degradation of the cationic photoinitiator without UV exposure.

Prior to photopolymerization, a similar film thickness of 15 μm was selected whatever the monomer. In a second step, alkoxysilane precursors were irradiated with an intensity of 180 mW/cm^2, leading in both cases to transparent and homogeneous films with a gel content of nearly 100%. In this study, we employed a diaryl iodonium salt (I 250) as a photoinitiator for both the organic and inorganic moieties. I 250 is well-known in the literature to be a very efficient cationic photoinitiator for the ring-opening polymerization of epoxy.[47] Scheme 1 outlines an idealized structure of the hybrid interpenetrating networks formed by simultaneous reaction of the inorganic and organic parts of TRIMO and GPTMS. The photolysis of the photoinitiator generates the very powerful superacid HPF_6, enabling two types of reaction:

(1) First, epoxy protonation takes place through a rapid and quantitative process. A series of chain-propagation then follows via epoxy ring-opening, affording a linear poly(ethylene oxide) (PEO).

(2) On the other hand, superacids are effective in catalyzing sol−gel reactions. The mechanism of the HPF_6-catalyzed reaction is similar to that of a conventional HCl-catalyzed process in solution. Basically, it proceeds as a two-step network-forming polymerization. Alkoxy functions (SiOR) are first hydrolyzed to generate silanol intermediate species (SiOH). These latter can then undergo a stepwise polycondensation reaction to form a three-dimensional silica network (Si−O−Si). In contrast to typical sol−gel process, there is no water in the present UV-curable system. Traces of water from air moisture

Scheme 1. Organic−Inorganic Hybrid Network Formed by the Dual Photo-Cross-Linking of GPTMS (A) and TRIMO (B)

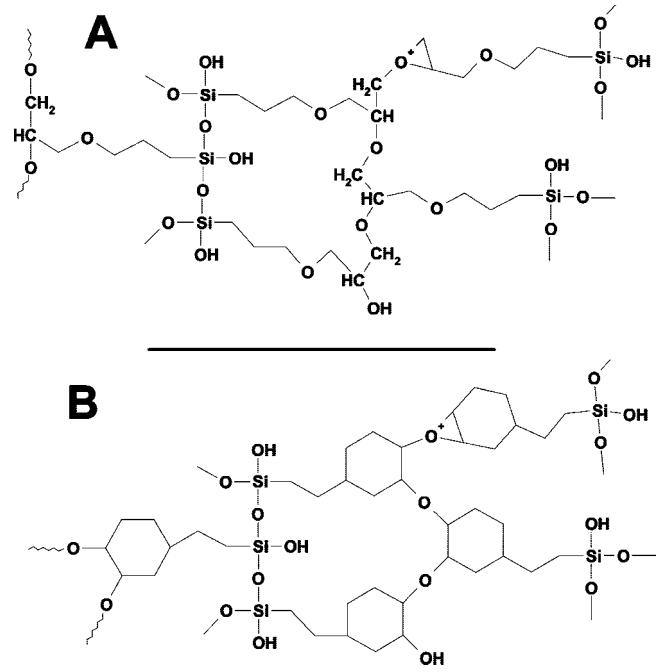

appear to be sufficient to initiate the hydrolysis reactions. The sol−gel polymerization of trialkoxysilanes such as TRIMO or GPTMS is known to result in the formation of polysilsequioxane (polySSQO) $(RSiO_{3/2})_n$ products denoted T_n.[48] PolySSQOs are generally described as a mixture of linear, branched and also cyclic polyhedral structures.

Other authors have studied the concept of ambifunctional monomer, but they all resorted to conventional acid or basic catalysts. Compounds such as (γ-aminopropyl)triethoxysilane,[49] BF_3[50] and various transition metal alkoxides[51] enabled both siloxane formation and epoxy ring-opening polymerization. However, their lack of latency prevented their practical application. In contrast to these methods, the use of cationic photoinitiator provides a convenient method of generating powerful acid catalysts in situ: the photoinduced organic−inorganic reactions can be triggered precisely by irradiation when desired, without processing and storage difficulties. Furthermore, UV technology obviates the difficulties of the sol−gel general process that starts in alcoholic solution including a catalyst and water. Last, photoacids are true catalysts which are not incorporated into the polymer microstructure.

RT-FTIR was found to be a very powerful technique to investigate the formation of the hybrid network as a function of the irradiation time. Figure 1A shows the RT-FTIR absorption spectrum of the GPTMS sample throughout the UV irradiation between 3700 and 3000 cm^{-1}. This spectral region assigned to O−H stretching vibrations evolves appreciably under UV irradiation. After only one second of UV treatment, a substantial increase in intensity is visible in conjunction with a shift toward lower wavenumbers, which can be attributed to the transition from isolated silanols (3700−3500 cm^{-1}) to hydrogen-bonded silanols (3650−3200 cm^{-1}).[52] Further exposition to UV light gives rise to a broad and intense band around 3400 cm^{-1} whose presence can be explained by the photoacid-catalyzed hydrolysis of SiOMe groups resulting in the formation of SiOH functions. Nevertheless, absorption intensity of this stretching region is not proportional to the hydroxyl group concentration since this band increases with hydrogen-bonding interactions. In such highly fluid precursors, water readily diffuses into the film to permit hydrolysis reactions. Other phenomena support this result:

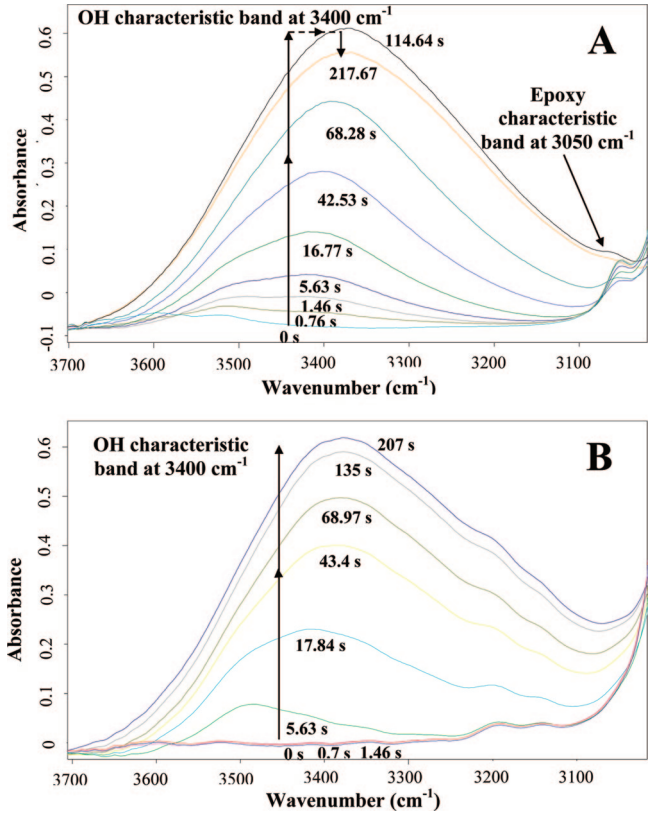

Figure 1. RT-FTIR spectra of GPTMS (A) and TRIMO (B) samples between 3700 and 3000 cm^{-1} throughout UV irradiation (light intensity 180 mJ/cm^2, 210 s, 15 μm).

the disappearance of the band at 2840 cm^{-1} characteristic of the methoxysilyl groups and a broadening peak around 910 cm^{-1} due to SiOH stretching vibrations. After 110 s of exposition, the broad band centered near 3400 cm^{-1} starts decreasing in intensity. This may be the sign of important condensation reactions of silanol groups followed by elimination of water or methanol molecules. In agreement with this, an intense peak appears at about 1100 cm^{-1} that was assigned to Si−O−Si asymmetric stretching vibrations. In addition, a slow decrease of the band at 3050 cm^{-1} attributed to the epoxy groups can be observed in the FTIR spectrum (Figure 1A). Besides showing the low reactivity of the glycidylether function of GPTMS, this last result brings the evidence that epoxy ring-opening occurs concomitantly and quantitatively with the photoinduced sol−gel process. As can be seen in Figure 1B, UV-irradiation of TRIMO led to similar results. First, the OH band rises dramatically upon UV exposure until it levels off without exhibiting a downward trend. Last, TRIMO does not display a clear absorption band at 3050 cm^{-1}.

Figures 2A and 2B show the conversion of epoxy functions and the extent of hydrolysis reactions respectively in the GPTMS and TRIMO samples. Epoxy conversion throughout the UV illumination was determined by monitoring the decrease in area of characteristic absorption bands. Without being quantitative, the ratio between the intensity of the OH band at 3400 cm^{-1} and that of a reference peak at 1193 cm^{-1} corresponding to Si−CH_2 stretching provides a normalized intensity, giving interesting insight into sol−gel reactions. As shown graphically, the type of hybrid monomer has a strong impact not only on the epoxy cationic polymerization but also on the sol−gel kinetics.

(1) The monomer bearing an epoxycyclohexyl group displays a much higher reactivity than that containing an epoxyether: conversion in epoxy from TRIMO reaches 90% after 6 s of

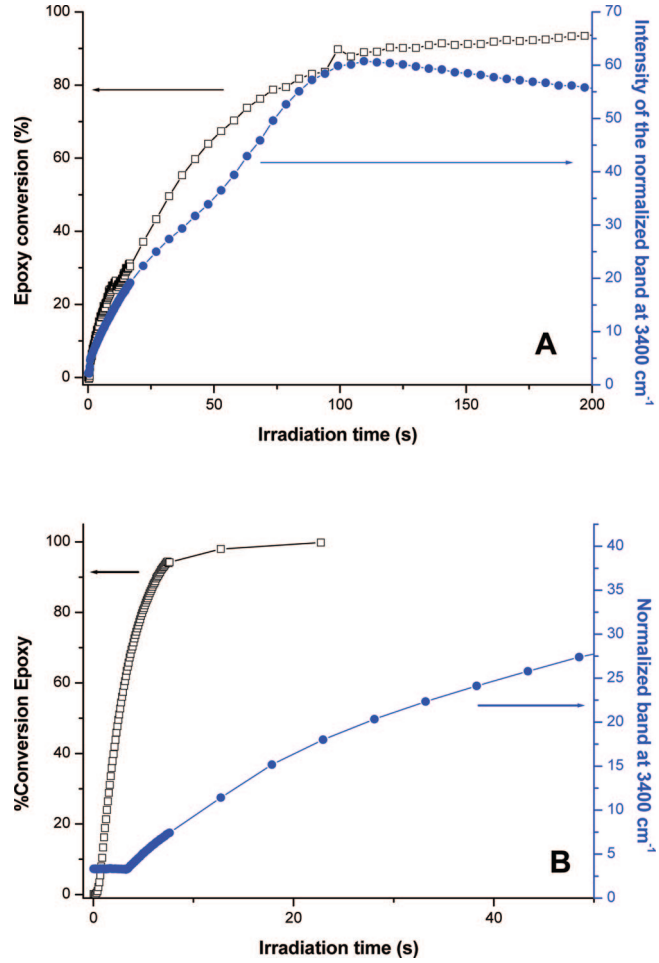

Figure 2. Epoxy conversion-time curve (left axis) and hydrolysis extent (right axis) monitored by the ratio between the intensity of the band at 3400 cm^{-1} and a reference peak at 1193 cm^{-1} during the cationic photopolymerization of GPTMS (A) and TRIMO (B) (light intensity 180 mW/cm^2, 210 s, 15 μm).

UV polymerization in contrast to 135 s in the case of GPTMS. Complete epoxy consumption was also achieved with this highly reactive precursor whereas a limiting conversion around 90% was observed with GPTMS. Three important factors, which are basicity, steric hindrance and ring strain, are known to contribute to the polymerizability of cyclic ether, irrespective of the type of initiating species.[53] The high energy of the ring strain in cycloaliphatic epoxies accounts for their high reactivity in acid-catalyzed ring-opening polymerization.

(2) GPTMS gives a valuable example of true concomitant organic inorganic UV-polymerization. In this case, sol−gel process and organic polymerization are catalyzed by photoacids in a synchronous way. TRIMO exhibits a very different behavior since hydrolysis becomes active subsequently to the reaction of the greatest part of the epoxy groups. Sign of absorbance at 3400 cm^{-1} indeed appears after 3.5 s when almost 70% of epoxy functional groups have been already converted. This would tend to suggest that UV curing of TRIMO proceeds in a stepwise manner: a poly(ethylene oxide)-based polymer including trialkoxysilyl functions was first synthesized before being subjected to sol−gel reactions.

(3) Presumably, the growth and decay of the OH concentration in the GPTMS sample are mostly governed by the relative importance of hydrolysis and condensation reactions throughout the irradiation time. At the early stage, the sol−gel process is thought to be mainly controlled by hydrolysis reactions, leading to an increased SiOH concentration. In a second step, condensa-

Table 2. Typical ^{29}Si NMR Signals of Silica Atoms Appearing in Oxo-Silica Structures Originated from Trialkoxysilanes

	T^0 sub-structure	T^1 sub-structure	T^2 sub-structure	T^3 sub-structure
δ_{Si} in ppm	-41 to -43	-48 to -52	-54 to -61	-64 to -69
Structure	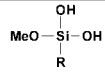	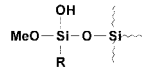	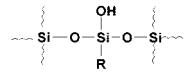	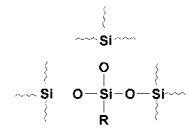

tion reactions become dominant over hydrolysis: silanol groups are thus consumed liberating water or methanol species. It is worthwhile to note that the transition from one stage to another provoked in this case a marked slowdown of the epoxy conversion rates. The odds are that a higher degree of condensation in the oxo-silica network will hinder the growth of the organic network. However, it is not obvious that all the volatile species liberated through condensation can be released out of the film. This might account for the different evolution of the OH band in the case of TRIMO. With this bulky monomer, the increased film rigidity is expected to favor water and methanol molecules' entrapment inside the coating.

II. Study of Hybrid Network Microstructure by ^{29}Si and ^{13}C NMR Spectroscopy. Solid state NMR spectroscopy has been implemented to investigate the structure of the hybrid material subsequently to the dual UV curing of GPTMS and TRIMO. Quantitative MAS NMR analysis was carried out in all cases with high power decoupling (HP/DEC) experiments. ^{29}Si MAS NMR is well-suited to the investigation of the structure of the oxo-silica. Table 2 summarizes the different environments at a silicon center (T^i) depending on the degree of condensation. In trialkalkoxysilane precursors, T^i indicates the fraction of the units with *i* siloxane bonds —O—Si— attached to the central silicon. Given all these substructures can be distinguished in a ^{29}Si NMR spectrum, one can have access to the degree of condensation in the siloxane network. ^{13}C MAS NMR is a complementary technique to investigate the organic part since the different opening reactions of epoxy rings can be distinguished.

II.1. Effect of the Photoacids on the Structure of the Oxo-Silica Inorganic Network. Figure 3A shows the solid state ^{29}Si NMR spectrum of a UV-cured GPTMS sample. It is interesting to note the absence of D^n or Q^n substructures, thus confirming that photoacids specifically attack alkosilyl functions like conventional Brönsted acids. The inorganic network was made up mainly of T^2 and T^1 siloxanes substructures, with a minor contribution from T^0 and T^3. Even though the network formed is not highly cross-linked, this clearly proves that UV-generated Brönsted acids are efficient in promoting sol—gel condensation reactions. For comparison, Figure 3A′ shows the liquid state ^{29}Si NMR spectrum of a GPTMS sol subjected to condensation for 72 h in a HCl aqueous solution (water to silicon ratio (r_w) = 3, pH = 1). Interestingly, the relative amount of T^2 in the UV-cured sample was found to be more than twice that obtained with a conventional sol—gel process. Upon replacing GPTMS by TRIMO, similar conclusions were reported (Figures 3B and 3B′). As observed previously, UV curing promotes a higher degree of condensation in the inorganic network: disubstituted siloxane linkages are mostly formed through a photoacid-catalyzed sol—gel process versus essentially monomeric species (T_0) in acidic solution. Nevertheless, such a result may seem surprising in the case of TRIMO given that the UV-generated inorganic network builds up subsequently to the formation of the organic photopolymer. Although the sol—gel step takes place in a viscous polymeric environment, being less permeable to water diffusion, a satisfactory cross-linking density can be achieved upon UV irradiation.

II.2. Effect of the Photoacids on the Structure of the Polyether Organic Network. Figures 4A and 4B display the ^{13}C MAS NMR spectra of the UV-polymerized GPTMS and TRIMO together with those of the unreacted precursors. Compared to the monomers, the UV-cured samples exhibit a broad and intense peak around 75 ppm readily related to the formation of oligo- or poly(ethylene oxide) chains via ring-opening reactions of the epoxy functions.[50] For TRIMO, the absence of signals corresponding to the carbons of the epoxy ring around 50 ppm is in itself the firm evidence that a complete opening of the epoxy has been accomplished. In contrast, residual epoxy groups at 44 ppm and 51 ppm remain in the GPTMS sample after the UV treatment. Although these ^{13}C MAS NMR experiments are quantitative, the peak at 51 ppm appears surprisingly larger than that at 44 ppm. This might be due to trapped methanol species (50.5 ppm) or incomplete

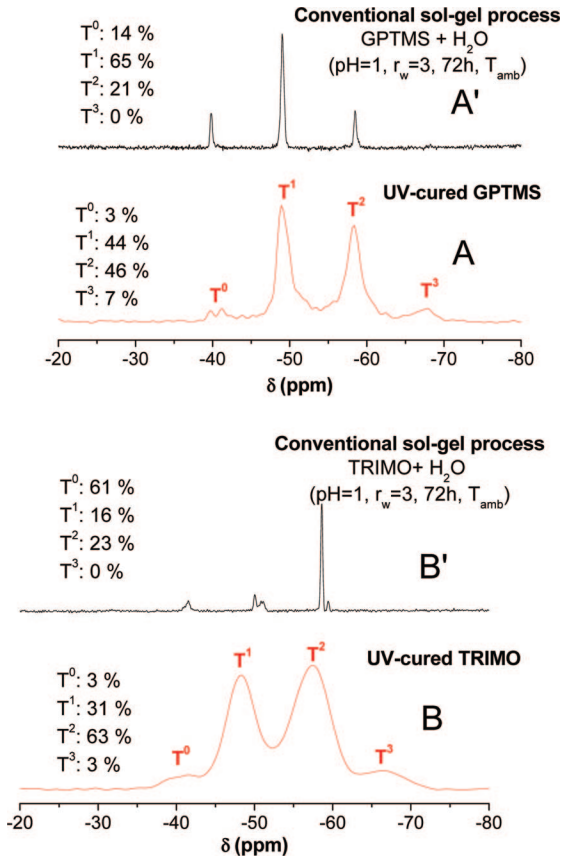

Figure 3. ^{29}Si Solid state MAS NMR spectra of UV-cured GPTMS (A) and TRIMO (B). For comparison, ^{29}Si liquid state NMR experiments were also recorded for the conventional sol—gel process of GPTMS (A′) and TRIMO (B′). Photopolymerization experiments were performed with a Minicure UV conveyor (10 passes, 3.3 J/cm^2 bypass, 15 μm).

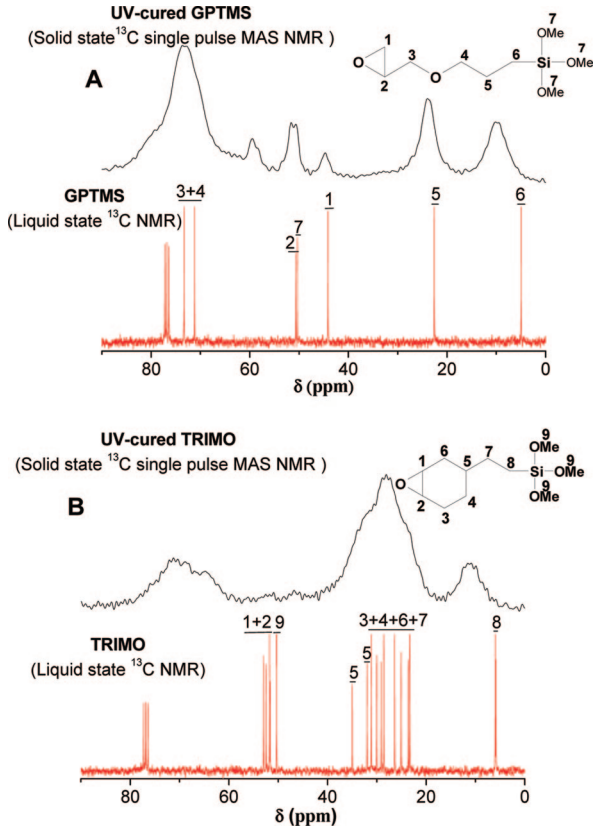

Figure 4. ^{13}C Liquid state NMR spectra of GPTMS (A) and TRIMO (B) before irradiation. For comparison, ^{13}C solid state MAS NMR spectra of the UV-cured organosilane monomers (A′, B′). Photopolymerization experiments were performed with a Minicure UV conveyor (10 passes, 3.3 J/cm^2 bypass, 15 μm).

Scheme 2. Nonproductive Side Reactions Leading to Epoxy Ring-Opening[a]

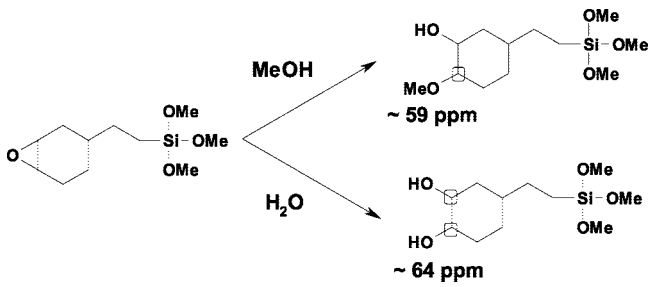

[a] Chemical shifts concern ^{13}C NMR.

hydrolysis since carbons of methoxy groups give a signal at 50.3 ppm. By comparing the smallest epoxy peak at 44 ppm with the reference signal given by the methyl groups located at 10 ppm, an epoxy conversion rate of 85% was estimated, which is in concordance with the result obtained by RT-FTIR (90%). In a view to be exhaustive, one must point out also the minor contribution of additional peaks at 59 ppm and 64 ppm originated by secondary epoxy ring-opening reactions,[54] as depicted in Scheme 2.

III. Influence of Experimental Conditions on the Organic−inorganic UV-Curing Kinetics. Sol−gel process and epoxy polymerization are known to depend on a number of experimental parameters. Some of them such as the film thickness, the type of substrate, and the reaction atmosphere were thus investigated in further detail.

III.1. Effect of Film Thickness. Cationic photopolymerization is not inhibited by ambient oxygen. For this reason, this process

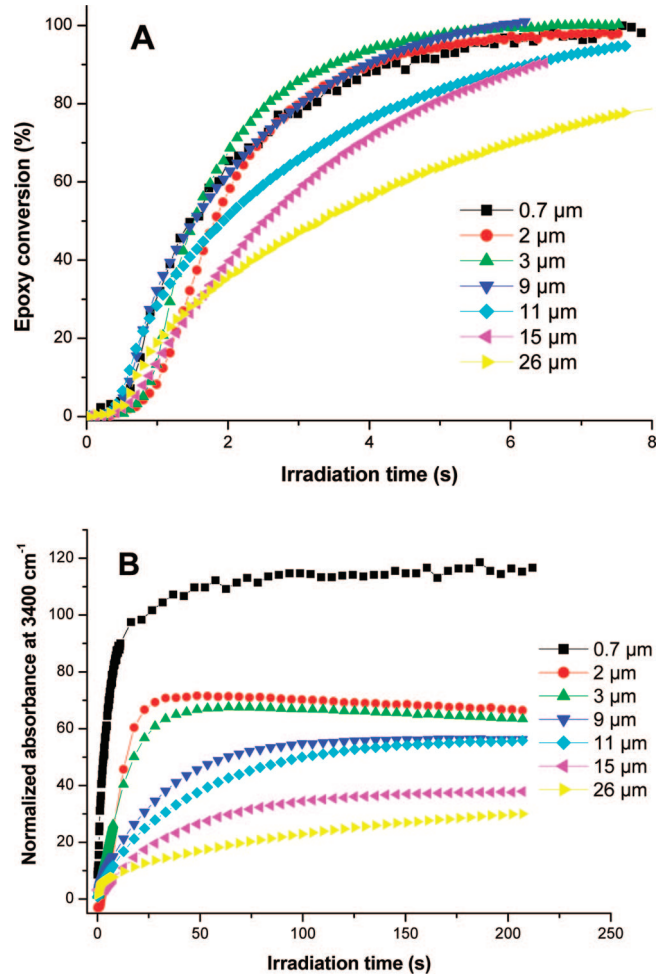

Figure 5. Influence of film thickness on epoxy conversion rates in GPTMS (A). Variation in intensity of the normalized band centered at 3400 cm^{-1} versus irradiation time for GPTMS samples with varying thickness (B). Light intensity = 180 mW/cm^2, 210 s.

is generally regarded as being much less dependent on film thickness than free-radical photopolymerization.[55] Although cationic photopolymerization of organic monomers and photoinduced sol−gel process of inorganic precursors both proceed by photoacid catalysis, two essential features distinguish the first type from the second one. The role of superacids is strictly limited to the initiation stage in an organic polymerization whereas the whole sol−gel process (hydrolysis and polycondensation) is acid-catalyzed. Another distinctive feature is the necessity of using water as a coreactant to initiate the hydrolysis reactions, unlike the case of classical cationic photopolymerization. Since the simple diffusion of water from air is responsible for the hydrolysis of trialkoxysilyl functions, it is obvious therefore that the film thickness will play an important role in determining the extent of the sol−gel reaction. It is thus expected that the thinner the film, the more readily water can diffuse throughout the whole film, hydrolyzing a higher number of alkoxy groups. Figures 5A and 5B show for TRIMO the effect of film thickness on the epoxy conversion profiles and the extent of hydrolysis reactions (intensity of the normalized band at 3400 cm^{-1}). The photoinitiator concentration being kept constant, the coating thickness was varied from 0.7 to 26 μm and its influence examined. As expected, hydrolysis is both accelerated and increased with decreasing film thickness. For the thinnest film at 700 nm, hydrolysis becomes even sufficiently rapid to occur simultaneously with the epoxy polymerization. Although the organic and inorganic polymerizations are now in competition for low film thickness, an accelerated sol−gel process does not

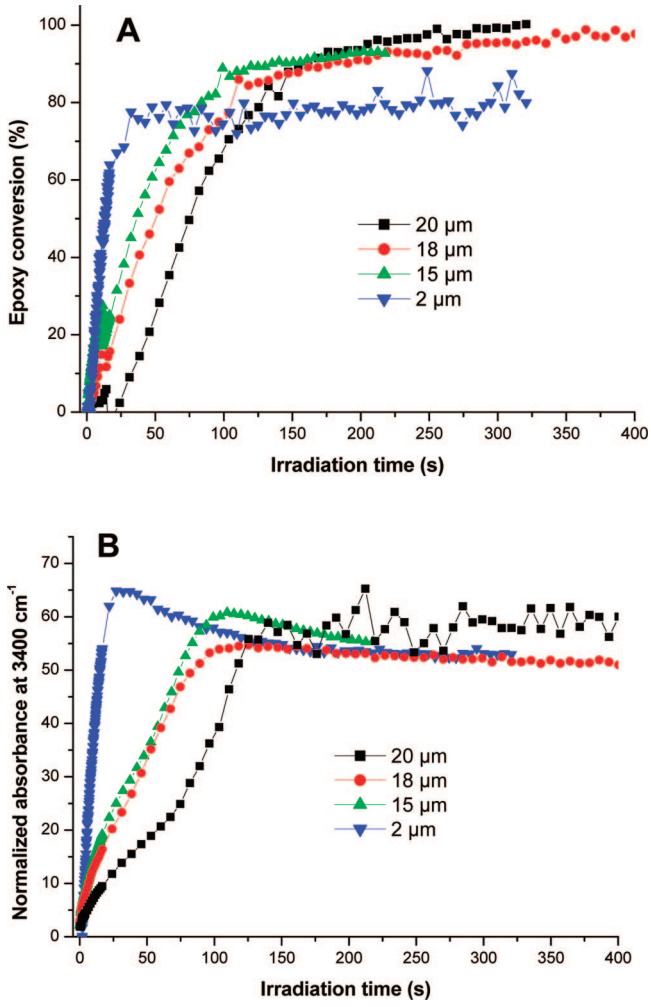

Figure 6. Influence of film thickness on epoxy conversion rates in TRIMO (A). Variation in intensity of the normalized band centered at 3400 cm^{-1} versus irradiation time for TRIMO samples with varying thickness (B). Light intensity = 180 mW/cm^2, 210 s.

provoke a decreased reactivity in epoxy conversion. On the contrary, a complete epoxy conversion is thus reached in less than 6 s of UV irradiation below 11 μm. With a thicker film, the rate of consumption of the epoxy becomes significantly slower and total epoxy consumption is now obtained after 25 s of illumination. In order to understand such a result, one must stress the possible participation of the silanol groups in the cationic ring-opening polymerizations. Crivello et al. recently reported that, in the presence of alcohol, the activated monomer (AM) mechanism is an effective means of accelerating the conversion of many types of epoxy monomers due to chain transfer reactions.[56] The influence of film thickness was also assessed when switching to a GPTMS precursor, as shown in Figure 6. As with the case of TRIMO, a decreased thickness results in a marked acceleration of the hydrolysis reactions. However, a similar evolution of the normalized absorbance at 3400 cm^{-1} was obtained during the UV irradiation whatever the film thickness, which is a major difference when compared to the TRIMO precursor. While the thinnest film of 2 μm turns out to be the most reactive, it has also a limiting conversion of 80%. In contrast, thicker films that proved to be less reactive showed a complete conversion. This might correspond to a situation where the silica network grows faster than the organic chains, thereby hindering sterically the epoxy-ring polymerization.

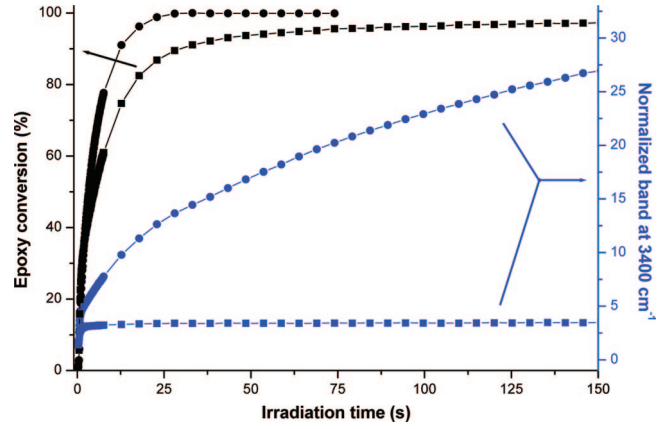

Figure 7. Evolution of the epoxy conversion (left axis) and hydrolysis extent (right axis) versus irradiation time in a TRIMO sample photopolymerized under air (●) and laminated conditions (■). Light intensity = 180 mW/cm^2, 210 s, 26 μm.

III.2. Effect of Atmospheric Water. (a) Comparison between Air and Laminated Photopolymerization. In a view to substantiate the major role played by air moisture in a photoacid-catalyzed sol−gel process, a series of experiments was performed with laminated samples. For this, a transparent polypropylene film was placed on top of the UV-curable film of 26 μm in order to prevent the diffusion of water into the sample, all other experimental parameters being kept constant. As illustrated in Figure 7, the sol−gel process is strongly inhibited under laminated conditions: the OH band increase is drastically interrupted after only 3 s of illumination, and then it levels off at very low values regardless of the exposure time. Presumably, this initial upward trend in OH groups is ascribed to limited hydrolysis reactions promoted by water initially dissolved in the sample composition. Once this water reserve has run out, henceforth further hydrolysis is precluded since atmospheric moisture is unable to penetrate into the sample. In agreement with this, only T_0 substructures were evidenced through NMR analysis, providing the conclusive evidence that condensation of Si−OR and Si−OH groups to form Si−O−Si bonds were efficiently hindered by the polypropylene top layer. Another interesting consequence is that water required for the sol−gel reaction must be obtained preferentially from atmospheric humidity.

Also shown in Figure 7 is a study of the organic polymerization conducted in a laminated composition of similar thickness. In this case, epoxy consumption proceeds very rapidly, with an initial reactivity $(R_p/[M]_0)_{max}$ value of 0.56 s^{-1} similar to that of a sample polymerized under air, as indicated by the slope of the conversion versus time. However, after 10 s illumination, both laminated and nonlaminated systems exhibit different kinetic behaviors. Although it is less sterically hindered because of the absence of inorganic network, the laminated sample displays more sluggish photopolymerization rates. This suggests once again the possibility for silanol groups to provide acceleration to the epoxy photopolymerization. In agreement with this, Crivello et al. proved that epoxy alcohol monomers well behave as monofers, resulting in more rapid photoinitiated cationic photopolymerization than analogous all-epoxy monomers.[57] In addition, Penczek et al. have demonstrated that in the presence of alcohols, the oxonium ion terminus of the growing polyether chain can react with the hydroxyl group of the alcohol.[58] Proton transfer reaction interrupts chain growth and generates a new propagating oxonium species. In a nonlaminated film, a higher hydrolysis extent generates a greater concentration of Si−OH functions (methanol is also liberated by condensation reactions) that can be involved in the afore-

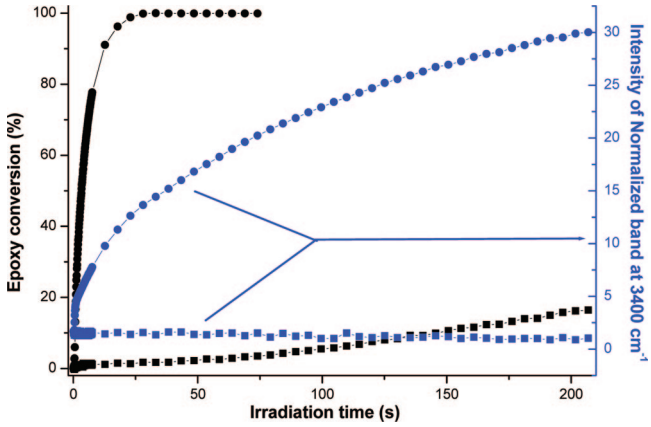

Figure 8. Photopolymerization of a TRIMO sample coated on a BaF_2 (●) and KBr (■) pellet. Effect of the substrate type on the organic and inorganic polymerization kinetics. [I 250] = 2 wt %, light intensity = 180 mW/cm^2, 210 s, 15 μm.

mentioned "activated monomer mechanism". This may be particularly advantageous in our case to provide a means for mobilizing the propagating cationic species that would normally be sequestrated within the glassy matrix of the cross-linked oxo-polymer that is formed.

(b) Comparison between Photopolymerization Performed on KBr and BaF_2 Substrates. In a last experiment, a photopolymerizable solutions including TRIMO was spread on KBr pellet instead of BaF_2. After ensuring the reproducibility of the sample thickness, the photopolymerization was triggered upon illuminating the sample. It is interesting to note that KBr disk was first discarded as IR transparent substrate for RT-FTIR measurements because it is known to be hygroscopic, in the sense that even small amounts of water liberated by sol−gel condensation reactions might dissolve the pellet and alter the quality spectrum. Conversely, its ability to absorb water was here advantageously exploited to perform a polymerization under anhydrous conditions. This will aim at completing our knowledge on the important role of water on the fundamental polymerization kinetics of epoxy and trialkoxysilyl functions. The results of the kinetic studies for TRIMO samples deposited on KBr pellet are depicted in Figure 8. Besides inhibiting totally the hydrolysis reactions, KBr resulted in a substantial decrease in both the rate of epoxy polymerization and the conversions. A remarkable 24-fold decrease in the rate of the photopolymerization of this monomer was observed when deposited on KBr. At the same time, the conversion of epoxy reaches less than 20% conversion after 200 s irradiation whereas only 5 s was normally necessary to achieve a complete conversion with a BaF_2 pellet. Such a result offers additional evidence for the participation of water directly in the photoinduced sol−gel process and indirectly in the epoxy photopolymerization mechanism.

IV. Thermal Characterization of Hybrid UV-Cured Films by Dynamic Scanning Calorimetry (DSC) and Thermogravimetric Analysis (TGA). Thermal stability of the hybrid sol−gel films obtained by UV-curing of TRIMO and GPTMS was evaluated by DSC and TGA analysis.

As depicted in Figure 9, DSC measurements carried out on similar hybrid materials did not display any distinct first or second order change generally attributed to phase transitions. This result is readily explained by the highly cross-linked structure of our hybrid films that strongly restricts chain mobility. On the first heating run, the sample yielded a broad endothermic peak with minimum at 83 °C for TRIMO and 79 °C for GPTMS. A thermal densification of the siloxane network is thought to occur at 50−100 °C. Softening of the cured

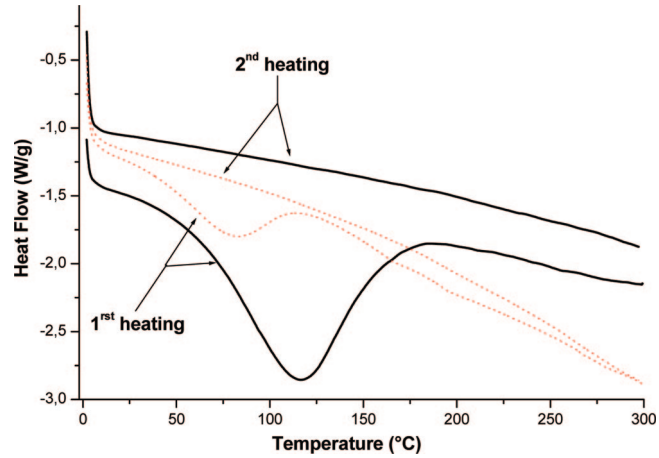

Figure 9. DSC thermograms of UV-cured GPTMS (···) and TRIMO (—).

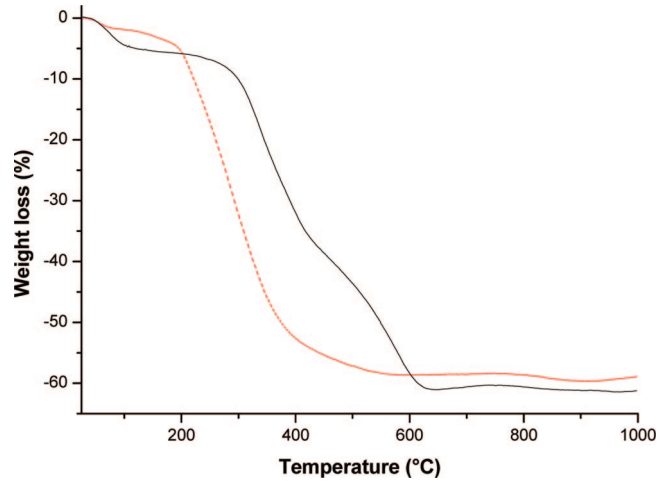

Figure 10. TGA spectra showing the variation of weight loss with temperature for UV-cross-linked GPTMS (···) and TRIMO (—).

material on DSC heating may facilitate new silanol condensation reactions and thus a thermal workup of the material. This proposal was confirmed by a second heating in which no endothermic peak was observed.

TGA analyses of similar samples provided complementary results on thermal stability of the hybrid samples (Figure 10). Decomposition of the UV-cured samples showed 3 temperature ranges. The first one at 25−200 °C corresponds to the removal of volatile species formed in the curing process or liberated by postconsolidation reactions. A marked weight loss is clearly visible for the TRIMO-based film during this first phase, providing another proof that volatile species trapped within the film could be released by TGA heating. For higher temperatures comprised between 200 and 600 °C, a significant sample weight loss was observed owing to the decomposition of C−O and Si−C bonds. Material based on GPTMS starts to decompose at lower temperature: 200 °C compared to 300 °C for UV-cured TRIMO samples. Rigid cyclohexyl groups are likely to increase substantially the macromolecular chain rigidity, thus improving the thermal stability. Moreover, the thermal decomposition occurs more slowly with a film based on TRIMO whereas a rather sharp disintegration was reported for its glycidylether analogue. Between 600 and 1000 °C, the overall trend for both materials was fairly steady. In both systems, a similar residue weight around 40% was recorded. This result reflects the fact that both precursors led to materials exhibiting comparable level of condensation. Finally, the stability of the sample weight over

high temperature may be consistent with the formation of oxycarbosilanes at the end of the process. As described in the literature, thermolysis of silsequioxane resins is known to afford silicon oxycarbide chars and silicon carbide ceramics.[39]

Conclusion

Onium salts are well-known for use in the chain photopolymerization of epoxy, vinyl ether and other cationically curable groups. Their utility in catalyzing the sol−gel process of reactive silanes has not been extensively recognized. In this work, we described the dual organic−inorganic UV-curing of ambifunctional hybrid precursors such as GPTMS and TRIMO, including both an organic epoxy function and a trialkoxysilane group. Dual UV curing implies that hybrid networks are prepared by simultaneous formation of inorganic and organic phases through the catalysis of photoacids formed by photolytic degradation of aryl iodonium salts. Traditionally, by using organically modified alkoxysilane, the organic network buildup occurs within a preformed liquid sol−gel inorganic network which imposes restrictions on the molecular movement. In this case, whatever the monomer implemented, remarkable epoxy conversion rates and high degree of condensation were achieved respectively for the organic and inorganic moieties. Both hybrid monomers displayed distinct kinetics profiles: while hydrolysis became active subsequently to the organic polymerization with a TRIMO sample, both processes occurred in a synchronous way with GPTMS. ^{29}Si NMR measurements also showed that UV curing advantageously promoted a higher degree of condensation in the inorganic network than a conventional sol−gel process in solution. For the organic moiety, the formation of poly(ethylene oxide) chains via ring-opening reactions of the epoxy functions was evidenced by ^{13}C NMR. By implementing experiments in laminated and anhydrous conditions, atmospheric water was found to play a major role on the activation of epoxy and alkoxysilane polymerization kinetics. Upon increasing film thickness, the photocatalyzed sol−gel reaction was strongly inhibited. Finally, the highly cross-linked structure of the hybrid films was characterized by DSC and TGA. In particular, rigid cyclohexyl groups substantially improved the thermal stability of the TRIMO-based sample compared to its epoxyether analogue (GPTMS).

References and Notes

(1) Rose, K.; Vangeneugden, D.; Paulussen, S.; Posset, U. *Surf. Coat. Int. Part B* **2006**, *89*, 41–48.
(2) Ajayan, M.; Schadler, L. S.; Braun, P. V. *Nanocomposite Science and Technology*, 1st ed.; Wiley-VCH: Weinheim, Germany, 2003.
(3) Schottner, G.; Rose, K.; Posset, U. *J. Sol-Gel Sci. Technol.* **2003**, *27*, 71–79.
(4) Amberg-Schwab, S.; Katschorek, H.; Weber, U.; Burger, A.; Haensel, R.; Steinbrecher, B.; Harzer, D. *J. Sol-Gel Sci. Technol.* **2003**, *26*, 699–703.
(5) Schottner, G.; Kron, J.; Deichmann, A. *J. Sol-Gel Sci. Technol.* **1998**, *13*, 183–187.
(6) Coudray, P.; Etienne, P.; Moreau, Y. *Mater. Sci. Semicond. Process.* **2000**, *3*, 331–337.
(7) Schwalm, R. *UV Coatings Basics, Recent Developments and New Applications*, 1st ed.; Elsevier: Amsterdam, The Netherlands, 2007; p 223.
(8) Croutxe-Barghorn, C.; Soppera, O.; Carre, C. *J. Sol-Gel Sci. Technol.* **2007**, *41*, 93–97.
(9) Brusatin, G.; Della Giustina, G.; Guglielmi, M.; Innocenzi, P. *Prog. Solid State Chem.* **2006**, *34*, 223–229.
(10) Sangermano, M.; Amerio, E.; Priola, A.; Di Gianni, A.; Voit, B. *J. Appl. Polym. Sci.* **2006**, *102*, 4659–4664.
(11) Gigant, K.; Posset, U.; Schottner, G.; Baia, L.; Kiefer, W.; Popp, J. *J. Sol-Gel Sci. Technol.* **2003**, *26*, 369–373.
(12) Muh, E.; Stieger, M.; Klee, J. E.; Frey, H.; Mulhaupt, R. *J. Polym. Sci., Part A: Polym. Chem.* **2001**, *39*, 4274–4282.
(13) Crivello, J. V.; Song, K. Y.; Ghoshal, R. *Chem. Mater.* **2001**, *13*, 1932–1942.
(14) Soppera, O.; Croutxe-Barghorn, C. *J. Polym. Sci., Part A: Polym. Chem.* **2003**, *41*, 831–840.
(15) Amerio, E.; Sangermano, M.; Malucelli, G.; Priola, A.; Voit, B. *Polymer* **2005**, *46*, 11241–11246.
(16) Crivello, J. V.; Mao, Z. *Chem. Mater.* **1997**, *9*, 1562–1569.
(17) Lee, T. Y.; Bowman, C. N. *Polymer* **2006**, *47*, 6057–6065.
(18) Bauer, F.; Mehnert, R. *J. Polym. Res.* **2005**, *12*, 483–491.
(19) Cho, J.-D.; Ju, H.-T.; Hong, J.-W. *J. Polym. Sci., Part A: Polym. Chem.* **2005***43*, 658–670.
(20) Vu, C.; LaFerte, O.; Eranian, A. *Eur. Coat. J.* **2002**, 64–70.
(21) Xu, G. C.; Li, A. Y.; De Zhang, L.; Wu, G. S.; Yuan, X. Y.; Xie, T. *J. Appl. Polym. Sci.* **2003**, *90*, 837–840.
(22) Posthumus, W. Ph.D. Thesis, Technische Universiteit Eindhoven, Eindhoven, The Netherlands, **2004**.
(23) Li, F.; Zhou, S.; You, B.; Wu, L. *J. Appl. Polym. Sci.* **2006**, *99*, 3281–3287.
(24) Li, G.; Ni, X. *Mater. Lett.* **2008**, *62*, 3066–3069.
(25) Decker, C. *Polym. Compos.* **2006**, 188–205.
(26) Inceoglu, F.; Dalgicdir, C.; Menceloglu, Y. Z. *PMSE Prepr.* **2006**, *95*, 329–330.
(27) Khanbabaei, G.; Aalaie, J.; Rahmatpour, A.; Khoshniyat, A.; Gharabadian, M. A. *J. Macromol. Sci., Part B: Phys.* **2007**, *46*, 975–986.
(28) Mariani, A.; Bidali, S.; Caria, G.; Monticelli, O.; Russo, S.; Kenny, J. M. *J. Polym. Sci., Part A: Polym. Chem.* **2007**, *45*, 2204–2211.
(29) Tan, H.; Nie, J. *Macromol. React. Eng.* **2007**, *1*, 384–390.
(30) Martins, C. R.; Almeida, Y. M.; Nascimento, G. C.; Azevedo, W. M. *J. Mater. Sci.* **2006**, *41*, 7413–7418.
(31) Pucci, A.; Bernabo, M.; Elvati, P.; Itzel Meza, L.; Galembeck, F.; de Paula Leite, C. A.; Tirelli, N.; Ruggeri, G. *J. Mater. Chem.* **2006**, *16*, 1058–1066.
(32) Sangermano, M.; Yagci, Y.; Rizza, G. *Macromolecules* **2007**, *40*, 8827–8829.
(33) Yagci, Y.; Sangermano, M.; Rizza, G. *Chem. Commun.* **2008**, 2771–2773.
(34) Fox, F. J.; Noren, R. W.; Krankkala, G. E. US Patent 4,101,513, **1978**.
(35) Sekiguchi, M.; Sugiyama, N.; Sato, H. US Patent 6,207,728, **2001**.
(36) Walters, R. W.; Stewart, K. J. US Patent 6,150,430, **2000**.
(37) Liu, J. J.; Leir, C. M.; Moore, G. G. I.; Sherman, A. A.; Everaerts, A. I.; Boulos, M. A. US Patent 6,204,350, **2001**.
(38) Wu, D.; Liu, J.; Dennison, K. A. US patent 6,719,422, **2004**.
(39) Kowalewska, A. *J. Mater. Chem.* **2005**, *15*, 4997–5006.
(40) Crivello, J. V.; Bi, D.; Lu, Y. *Macromol. Symp.* **1995**, *95*, 79–89.
(41) Soucek, M. D.; Johnson, A. H.; Meemken, L. E.; Wegner, J. M. *Polym. Adv. Technol.* **2005**, *16*, 257–261.
(42) Zou, K.; Soucek, M. D. *Macromol. Chem. Phys.* **2004**, *205*, 2032–2039.
(43) Amerio, E.; Sangermano, M.; Malucelli, G.; Priola, A.; Voit, B. *Polymer* **2005**, *46*, 11241–11246.
(44) Amerio, E.; Sangermano, M.; Malucelli, G.; Priola, A.; Rizza, G. *Macromol. Mater. Eng.* **2006**, *291*, 1287–1292.
(45) Sangermano, M.; Amerio, E.; Epicoco, P.; Priola, A.; Rizza, G.; Malucelli, G. *Macromol. Mater. Eng.* **2007**, *292*, 634–640.
(46) Massiot, D. *J. Magn. Reson.* **1996**, *122*, 240–244.
(47) Fuchs, A.; Ilg, S.; Bolle, T.; Birbaum, J. L. *Ink Maker* **2002**, *80*, 48–50.
(48) Matejka, L.; Dukh, O.; Hlavata, D.; Meissner, B.; Brus, J. *Macromolecules* **2001**, *34*, 6904–6914.
(49) Riegel, B.; Blittersdorf, S.; Kiefer, W.; Hofacker, S.; Muller, M.; Schottner, G. *J. Non-Cryst. Solids* **1998**, *226*, 76–84.
(50) Innocenzi, P.; Brusatin, G.; Babonneau, F. *Chem. Mater.* **2000**, *12*, 3726–3732.
(51) Hoebbel, D.; Nacken, M.; Schmidt, H. *J. Sol-Gel Sci. Technol.* **1998**, *12*, 169–179.
(52) Innocenzi, P. *J. Non-Cryst. Solids* **2003**, *316*, 309–319.
(53) Penczek, S.; Kubisa, P. *Comprehensive Polymer Science*; Pergamon Press: Oxford, New York, Beijing, 1989; Vol. *3*.
(54) Templin, M.; Wiesner, U.; Spiess, H. W. *Adv. Mater.* **1997**, *9*, 814–817.
(55) O'Brien, A. K.; Bowman, C. N. *Macromolecules* **2006**, *39*, 2501–2506.
(56) Crivello, J. V.; Ortiz, R. A. *J. Polym. Sci., Part A: Polym. Chem.* **2002**, *40*, 2298–2309.
(57) Crivello, J. V.; Liu, S. *J. Polym. Sci., Part A: Polym. Chem.* **2000**, *38*, 389–401.
(58) Penczek, S.; Kubisa, P.; Szymanski, R. *Makromol. Chem., Macromol. Symp.* **1986**, *3*, 203–220.

MA801017K